Study of the Electronic Charge Distribution for a Structural Configuration of the Liquid Silica Through Classical and ab-initio Molecular Dynamic Simulations

G. Lopez-Laurrabaquio, M. E. Fernandez-García, J. M. Montejano-Carrizales, C. Díaz Torrejon

Abstract— A combination of classical and ab-initio molecular dynamics computer simulations will be done to a system of silica atoms in order to generate a structural configuration in the liquid phase. In the first method, the effective classical potential (B. P. Feuston and S. H. Garofalini, J. Chem. Phys. **89**, 5818 (1988)) and in the second one, the pseudopotencials of N. Trouiller and J. L. Martins (N. Trouiller, J. L. Martins, Phys. Rev. B **43**, 1993 (1991)), will be used. We will begin by melting one of the crystalline silica forms, beta cristobalite, to 3400 K and then it will be permitted to acquire a thermal equilibrium (equilibration) at this temperature; all of this will be done with classical molecular dynamic simulations. Later we will cool it at 2200 K, in order to obtain that we will perform a strategic and systematic combination of two methods. In the stage of the equilibration and cooling to the system will be placed in a geometric arrangement denominated "sandwich", which will generate a surface-type structural configuration. This form of obtaining the surface will permit to make ab-initio calculations in a way that the properties of the surface can be analyzed in a detailed form.

Index Terms—ab-initio molecular dynamics, beta cristobalite, charge distribution, SIESTA.

1 Introduction

The silica (SiO_2) is a material that possesses unusual properties in its different phases: liquid, crystalline and vitreous[1], for example, its innocuousness, its diverse crystalline polymorphs, the amorphous and insulating nature, and the glassy transition temperature. This makes the material important for scientific investigation and a great interest in its applications: in the microelectronic, catalysis and recently, in medicine[2]. Therefore, it is necessary to have a better understanding of this material. It is relevant to indicate that the classical and ab-initio molecular dynamics (MD) computer simulations have demonstrated that the structural and dynamic properties of the SiO_2 in its respective phases can be reasonably well simulated and can provide details of atomic level behavior not normally observable though the experimental techniques[3],[4].

The classical molecular dynamic simulations in conjunction with an effective classical potential[5] have described the properties of bulk amorphous silica and the vitreous silica surface[6], with a good concordance with the experimental data. Recently some studies of the amorphous silica surface have been done combined classical and ab-initio MD simulations. The classical simulation uses the effective classical potential, such as, the one proposed some years ago by van Beest, Kramer, and van Santen (BKS)[7] and the ab-initio simulation uses the pseudopotentials implemented in the CPMD[8] code. The reason of using this combination is because the classical potential was designed to reproduce the bulk silica properties and it is less obvious that it can be used in aspects to study the surface. Also, the simulation time and the number of particles are greater in the classical than in the ab-initio[9] simulation.

On the other hand, a supercooled liquid[10],[11] (a liquid with high viscosity) whose constitutive material, for example the silica, when cooling is being applied a great cooling velocity in a way that the crystalline state is inhibited, tends to a glassy transition temperature, T_g, where the structural configuration gets "trapped". Above T_g, metastable region, the supercooled liquid can explore all the structures or configurations at equilibrium (metastable state), since the relaxation times for the molecular movements are very short compared to the experimental timescale[12]. So, these times stay within the timescale of the simulations. However, under this temperature, off-equilibrium region, for the system to reach a stable state of equilibrium an excessively considerate time would be needed so that the time scale of the experiment or simulation would not to be enough

- *G. Lopez-Laurrabaquio, Depto. de Física, Instituto Nacional de Investigaciones Nucleares, Edo. de México, México, citecgllapril@yahoo.com.mx*
- *M. E. Fernandez-García, Depto. de Tecnologia de Materiales, Instituto Nacional de Investigaciones Nucleares, Edo de México, México. maria.fernandez@inin.gob.mx*
- *J. M. Montejano-Carrizales, Instituto de Física de la Universidad Autónoma de San Luis Potosí, San Luis Potosí, México. jmmc@ifisica.uaslp.mx*
- *C. Díaz-Torrejon, Laboratorio Nacional de Supercomputo del Sureste de México, Benemérita Universidad Autónoma de Puebla, Puebla, México*

for the time of the relaxation[10]. It is interesting to note that the structural configuration of the liquid and vitreous phase is identical[13],[14]. That is why it is important and necessary to make a deeper and more detailed analysis in its quantum properties, for example the electronic density of states (DOS) and electronic charge distribution in each of the atoms that constitute the system.

Our work will be about the study of the quantum properties of the surface (in liquid phase) through a combination of the classical and ab-initio MD simulations, in a systematic and strategic way. In the classical simulation, the effective classical potential[5] will be used, performing it in the LAMMPS[15] code, and the ab-initio simulation with pseudopotentials of N. Trouiller and of J. L. Martins[16] through the SIESTA[17],[18] code. This second code is more efficient and versatile compared to the CPMD. The SIESTA possesses the Voronoi Deformation Density (VDD) method[18],[19] for computing atomic charges, for each of the atoms of the system. This method performs an equipartition of the space (Voronoi polyhedron) where each of the atoms that form the system are located. And, the analysis is independent of the form of the base set used to expand the corresponding wave functions. This code will also permit us analyze the topological and bond defects between atom pairs for all the system.

This article is divided in the following way. The section 2 expresses the standard MD melt-quench technique; in the subsection 2.1, the procedure of melting the β-cristobalite to 3400 K; in the subsection 2.2, the setup of the geometry (sandwich) and equilibration of the silica liquid phase at this temperature (3400 K); and in the subsection 2.3, the quenching of the liquid phase to 2200 K (using the combination of both methods, classical and ab-initio, in a systematic and strategic way; the second method to calculate the DOS, electronic charge distribution, topological and bond defects, to different temperatures that the system passes through while it tends to a T_g). In the section 3, the details of the parameters of these two computer codes are described. In the section 4, the results and discussion are presented. At last, in the section 5, conclusions are enumerated.

2 The Standard Molecular Dynamics Melt-Quench Technique

2.1 Melting

The atoms are initially assigned random velocities through a Maxwell-Boltzmann distribution associated to the temperature of 3400 K and use an initial configuration to one of the crystalline structures of the silica (cristobalita beta with 192 atoms). The simulation was performed in a microcanonical ensemble (NVE, number of atoms, volume and energy are constants) with periodic boundary conditions (PBC) in the three directions X, Y and Z, to avoid the effects of the internal surface, the volume of the simulation cell of the MD simulation was chosen in a way that the density adjusts the temperature in question. It is important to mention that the volumetric dilatation of the β-cristobalite is almost despicable in a great interval of temperatures, this temperature is in this range[20]. The time step of the simulation was of 0.001 ps (see section III). The initial configuration was melted at 3400 K by periodic velocity scaling during the first 30,000 MD time steps. Therefore, when the melting of this configuration is obtained, the next stage proceeds.

2.2 The Setup of the Geometry (Sandwich) and Equilibration

The way to minimize finite size effects and the superficial effects is using the PBC in the three directions. If one wishes to analyze a free surface, the immediate idea is to use a film geometry, i.e. to have PBC in two directions and to have an infinite free space above and below the system. Unfortunately, from the computer point of view this arrangement is not good for systems with Coulombic interactions (that is, like the one that is being studied here) since it impedes the efficient use of the Ewald summation method. Therefore, we have utilized the following strategy, which is drawn in fig. 1 (a) (also see [6], [9], and [21]):

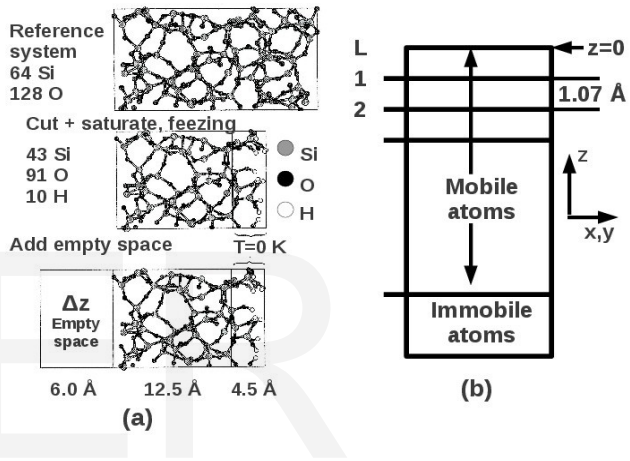

Fig. 1. (a) Procedure to create the sandwich geometry used; (b) A surface where the layers and their dimensions are described and mobile and immobile atoms are shown.

The construction of the geometric arrangement denominated "sandwich" is done as Mischler[9] describes it, with some small changes; like the hydrogen electronic charge, +1.0, and the longitude of the simulation box in the z-direction, L_z, 23 Å. This is due to the Feuston potential, described in detail in [5], combines a weak three-body interaction with a modified Born-Mayer-Huggins ionic pair interaction, and the electronic charges used in this potential are +4 and -2 for a silicon and oxygen atom, respectively; Mischler uses the BKS[7] potential, where the effective charges of a silicon and oxygen atom are +2.4 and -1.2, respectively. Besides, the three-body contribution lowers the total binding energy when the angle formed by a central atom and two of its covalently bonded neighbors differs from the perfect tetrahedral angle.

Proceeding, will be used the classic system previously described, which will be equilibrated through the contact with a heat bath at 3400 K. The contact with heat bath is simulated using the stochastic collision method[22] with an average of 1 collision/fs for the whole sample. This temperature is above the experimental melting point of all the silica poliforms. The total time of the simulation is one nanosecond. This time is enough to equilibrate the system completely[23].

Carrying out a set of m-runs of this type of simulation, as a

result, final statistically independent m-configurations will be obtained, the value of m varies in some dozens (for example m=50). From this set of final classical configurations (surfaces), we notice the same as Mischler[9], in each of these surfaces is present one of the situations mentioned by them: systems with no defects (i. e. all Si and O atoms are four- and two-coordinated, respectively), and systems with an under-coordinated (over-coordinated) oxygen atom and an under-coordinated silicon (oxygen) atom.

2.3 Quenching

We will take 10 structural configurations, each one having the characteristics mentioned above; with each one of the selected will be implemented the systematic and strategic combination, to carry out the cooling of the liquid phase of the silica by means of the LAMMPS and SIESTA code, respectively. As will be next described:

First, each system was cooled by periodic velocity scaling in 200 K (temperature interval) decrements from 3400 to 2200 K, reaching internal equilibrium at each intermediate temperature. At every temperature, the atomic velocities were scaled for the first 45.45 picoseconds (applying a lineal annealing through LAMMPS, with a time step of 1 fs; the cooling rate used is $4.4x10^{12}$K/s). Subsequently, with the last resulting configuration of the "actual" annealing a MD simulation is implemented at constant energy (and at the "final" temperature of this interval) using the LAMMPS code, the total simulation time of MD will be the same as the structural relaxation time (similar to the relaxation time of the coordination defects[24]) of the surface at the corresponding temperature. At the end of this annealing-relaxation cycle a final structure will be obtained, which we will denote by "α_i". This structure α_i is used in the following cycle. Performing all the prior in sequential manner, a temperature of 2200 K will be reached and the final configurations α_i (i=1,…,6) will be obtained. It is important to mention that in the succession of these cycles, in each one of them, finalizing the annealing process the box dimensions are adjusted in order to obtain the associated density to the temperature in question; although the adjustments of the dimensions are despicable due to the insignificant value of the volumetric dilatation of the SiO_2. Also, the same geometric strategy is used as expressed in the subsection 2.2.

At last, having the system at a temperature of 2200 K (after having applied a relaxation to this temperature), the SIESTA code is proceeded to apply with a total time of simulation of 0.27 picoseconds and with a time step of 0.1 fs, to realize the calculus of the electronic density of states, electronic charge distribution, topological and bond defects, to each of the final structure α_i; in each of the selected temperatures that the system went through until reaching the glassy transition temperature (T_g= 2200 K, theoretic value[13] and for this cooling rate $4.4x10^{12}$ K/s). The results of these ab-initio calculations are presented in section 4.

3 LAMMPS and SIESTA Simulation

3.1 LAMMPS Code: The Classical Molecular Dynamic Simulation (Classical Simulation)

The Verlet[25] algorithm was used for integrating Newton's 3N equations of motion (N is the number of particles). However, because of the sharp curvature of the silicon-oxygen potential, it is necessary to perform a short time step of $1x10^{-15}$ seconds, which will be used to effectuate an exact numeric integration[26]. In this scheme, the expressions for the positions of the atoms (and the velocities) are in function of the acceleration, which is obtained through the gradient of the Feuston potential[5]. It is important to mention that this simulation is effectuated in a microcanonical ensemble (NVE constants). This algorithm will be used in the melting and relaxation process, with the condition of that each scaling was restricted so that the velocities did not increase more than 10 % upon heating or decrease more than 3 % upon cooling. In addition, considering the external pressure, p_{ext}, equal to zero. On other hand, in the lineal annealing a rescaling of the velocities will be used in each time step, and adjusting them to the target temperature, using the potential mentioned before.

3.2 SIESTA Code: The ab-initio Molecular Dynamic Simulation (ab-initio simulation)

For the SIESTA, we used conventional pseudopotentials for silicon, hydrogen and oxygen and the PBE and LYP exchange-correlation functionals[16],[27], respectively. The electronic wave functions were expanded in a plane wave basis set with an energy cutoff of 160 Ry and the equation of motion were integrated with a time step of 0.1 fs for 0.27 picoseconds. It is relevant to mention that in this code it is enough to realize a number of interactions from 8 to 12 (depending on the number of particles in the system) in the field of selfconsistency associated to the equations of Kohn-Sham and implementing the pseudopotentials in the ab-initio calculus[17],[28]. This makes that the calculations in the simulations of the ab-initio MD be relatively quick and exact, because of how the SIESTA[17] was constructed. It is important to mention that the calculation of the electronic density of states, electronic charge distribution, and topological and bond defects, all of them are calculated at the end of the running (that is after the last iteration of the self-consistent cycle and for the final geometry). In an analogous way, as the classical molecular dynamic is considered p_{ext}= 0.

4 Results and Discussion

To each and every one of the surfaces α_i's (obtained in the section 2) are applied the SIESTA code within a microcanonical ensemble, and at the end of each run the electronic and structural properties were calculated. Each of the α_i's have 103 mobile atoms and 41 immobile in a simulation cell approximately 11.51x11.51x23 $Å^3$ thick. The structure of each of these surfaces was then studied in detail, with particular attention to the type and number of defects, e.g. topological defects such as two-, three-, and four-membered rings[29], and bond defects as determined by the presence of under- or over-coordinated atoms. Also, the electronic density of states and electronic charge distribution were analyzed. Two ratios of 2.0 and 2.5 Å were used as cutoffs, R_c's, for defining the nearest-neighbor shell about each atom with the number of bonds corresponding to the number of atoms within this shell. For the analysis and discussion of the results, each surface was analyzed in rectangular volume elements (layers) parallel to the surface. The topmost

layer corresponds to the z boundary of the mobile atoms and we put z= 0 Å on the outermost atom (that in general is an oxygen atom) while the subsurface layers are assigned negative z values. The defects were analyzed in terms of the individual layers L_{m+1}, corresponding to the rectangular volume element whose lower and upper faces were located at –(m+1) (1.07) and –(m) (1.07) Å, respectively (with m=0,…,6, see fig. 1 (b)). The effect of the arbitrarily chosen layer thickness (1.07 Å) on the results presented below have been minimized by averaging over the 10 different surfaces corresponding to the regarding α_i. We will denote this statistical process as "average surface" A_i. Next the results the bond defects will be presented associated to each one of the A_i's (i= 1,…, 6).

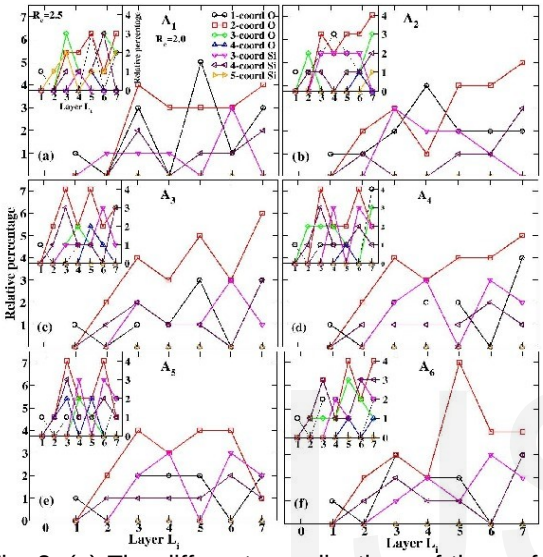

Fig. 2. (a) The different coordinations of the surface A_1 associated to the R_c= 2.0 Å showed in the main figure, as well as, the relative percentages in each of the layers (L_i's); in the inset for the associated to the R_c= 2.5 Å. In a successive manner to figure (f).

In the A_1 and A_2 (fig. 2) is observed in the main figures that in the layer 1, L_1, the influence of the nonbridging oxygen (NBO)[30], one-coordinated oxygen, in the following layers the under-coordinated oxygen and silicon are present in notable percentages. However, for R_c=2.5 Å (inset) it can be noticed that in the initial and intermediate layers the influence of the over-coordinated oxygen and silicon (in less amount for this last element) and also reasonable percentages of under-coordinated silicon. Also, the percentage of two-coordinated oxygen is more than the four-coordinated silicon. It can be observed that the amount of oxygen atoms is higher than that of the silicon in each layer. For A_3, again the predominance of the nonbridging oxygen at the beginning, in the intermediate layers the influence of the under-coordinated silicon can be noticed the same as of the over-coordinated oxygen, it is again notorious more percentage of two-coordinated oxygen than four-coordinated silicon. Now for A_4, a presence of under- and over-coordinated oxygen can be visualized at the beginning, in the intermediate layers appreciable percentages of over-coordinated oxygen and under-coordinated silicon, but also percentages of the nonbridging oxygen (in the different layers). Furthermore, the appearance of a relation of percentages between two-coordinated oxygen regarding a four-coordinated silicon (approximately 2 to 1, respectively). For A_5 is very similar to A_4. Finally, for A_6, in the layer L_1 the existence of nonbridging oxygen, in the intermediate layers a greater percentage of under- and over-coordinated oxygen regarding the under-coordinated silicon. In some layers, the percentage of two-coordinated oxygen is the same as a four-coordinated silicon, but in the L_7, the relation 2 to 1 of the these previous coordinations is established. In all A_i's the number of atoms of oxygen is greater (or almost the same) than the ones of silicon for all the layers.

From the prior analysis of each of the layers for the A_i's and of the experimental and theoretical[6] interest we will focus on studying in the three first superior layers the electronic charge distribution of each atom that conforms the bond defects representative in each one of them. In the layer 1, the nonbridging oxygen; in the L_2, the three-coordinated silicon; and in the L_3, the three-coordinated oxygen (see fig. 3). All in function of the A_i's. Next these results are presented:

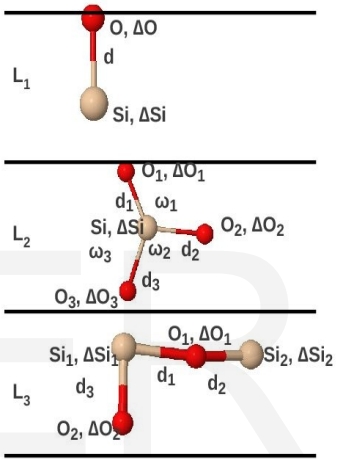

Fig. 3. In the layer 1, L_1, the nonbridging oxygen is shown (NBO), the atom of oxygen (O) more external and the silicon (Si) bounded to it. At the side of each symbol that represents the atom, is the variation of the corresponding electronic charge, Δ. The symbol d represents the longitude of the bond. For the L_2, the three-coordinated silicon is indicated and the same notation is used as in the L_1, the ω_1 represents the angle between O_1-Si-O_2, in an analogue manner for ω_2 and ω_3. In the layer L_3, the three-coordinated oxygen is shown and the notation is the same that was previously used.

For L_1, in the different A_i's are observed (see table 1), that the charge variation for oxygen is an excess of electrons, if it is compared with the other atoms of the other layers. However, the deficiency in electrons for silicon is similar to the ones of the other layers. (It should be mentioned that the variation of the electronic charge is the total net charge, Δ, of the atom: the variation from the neutral charge, in units of |e|: positive (negative) values indicate deficiency (excess) of electrons in the atom). The shrinking of the Si-O interaction distance for the different A_i' s is notorious (the bulk value is 1.62 Å). For the L_2, we notice a slight elongation of the Si-O bond, indicative of strain[6]. It can also be observed that the angles ω_1, ω_2 y ω_3 are in the interval variation (expressed in [31], for the bulk case). It is interesting to notice that starting from the A_4, the angle ω_1 tends to the two-membered ring (vitreous silica surfaces[6]) and angles ω_2 and ω_3 tend to the angles of the three-

and four- membered rings, respectively (amorphous silica surface[9]), in a similar way the magnitude of the Si-O bonds tends to their corresponding in these rings[6],[9]. We can see that the electronic charges ΔO_1 y ΔO_2 are almost identical starting from A_4. Finally, for the L_3, we observe that the lengths of the Si-O bond are in the range of the variation of the associated values to the bulk[31] case. It is also noticed that atoms that are "further away" from the O_1 (taken as a reference in this coordination) possess greater negative charge, as it is for the O_2, or greater positive charge, as it is for Si_2; unlike of the near atoms to O_1, as it is for Si_1. This makes us think that the further away atoms interact with others, which permits them to increase or diminish its charge, depending which is the corresponding atom.

Table 1. The values associated to each one of the physical quantities indicated in the fig. 3, in function to the average surfaces A_i's. The value of d is expressed in Å, the variation of the electronic charge, Δ, in units of |e| and ω in grades, see text.

	cycle	A_1	A_2	A_3	A_4	A_5	A_6
NBO	d	1.66	1.57	1.51	1.58	1.6	1.5
	ΔO	-0.23	-0.43	-0.47	-0.48	-0.4	-0.43
	ΔSi	0.55	0.5	0.52	0.51	0.55	0.57
3-coordinated silicon	d_1	1.66	1.6	1.69	1.72	1.76	1.58
	d_2	1.76	1.69	1.69	1.75	1.78	1.71
	d_3	1.84	1.69	1.72	1.83	1.79	1.98
	ω_1	105	105.1	102.4	90.1	88.8	96
	ω_2	117	119.7	107	117.6	114.6	102.7
	ω_3	133.8	134.4	109.3	117.7	117.4	131.3
	ΔO_1	-0.23	-0.23	-0.22	-0.25	-0.27	-0.29
	ΔO_2	-0.34	-0.29	-0.24	-0.27	-0.27	-0.3
	ΔO_3	-0.37	-0.37	-0.32	-0.3	-0.29	-0.34
	ΔSi	0.55	0.6	0.63	0.62	0.62	0.63
3-coordinated Oxigen	d_1	2.31	1.63	1.55	1.68	1.75	1.58
	d_2	1.84	1.75	1.62	1.89	1.78	1.76
	d_3	1.6	1.9	1.71	1.72	1.81	1.97
	ΔO_1	-0.2	-0.24	-0.2	-0.25	-0.27	-301
	ΔO_2	-0.37	-0.31	-0.24	-0.3	-0.29	-0.3
	ΔSi_1	0.55	0.5	0.58	0.51	0.55	0.57
	ΔSi_2	0.66	0.62	---	0.62	0.62	0.63

Now, we will analyze the topological defects according the A_i's and we will focus on the two- and three-membered rings, due to its experimental and theoretical importance. In the case of the two-membered ring, there are two different structures in the superior layers (see figure 4). At the top, the axis system, the "real" position and the layers that comprise this ring are indicated, likewise, the torsion of the structure (which is described by plane Si_1-O_1-O_2 and being outside Si_2 of this one by a torsion angle θ), showing that it is not coplanar. The left side, show the rotated structure, the magnitude of the Si-O bonds and the Si-O-Si interaction angles; the right side, indicate the variation of the electronic charges of each one of the atoms. It is interesting to note that when the oxygen charges (in an analogous way for the silicons) are relatively identical the structure is a "parallelogram", fig 4 (a), and in a contrary case, the form is "irregular" (see figure 4 (b)). Besides, these structures appear until A_6, and that is because this structural configuration requires a great of torsion energy for its creation, this energy is supplied through the annealing-relaxation process; likewise, the system in A_6 gets closer to the T_g. For the case of the three-membered ring can be correlated with the three-coordinated oxygen, if one considers the O_1 of the figure 4 (c) as the reference atom and considering table 1, we can see that there is a correlation between the electronic charges and the magnitudes of the Si-O bonds of this coordination and the three-membered ring, respectively. This is according to results of the literature[6]. In addition, this ring began to appear from A_4.

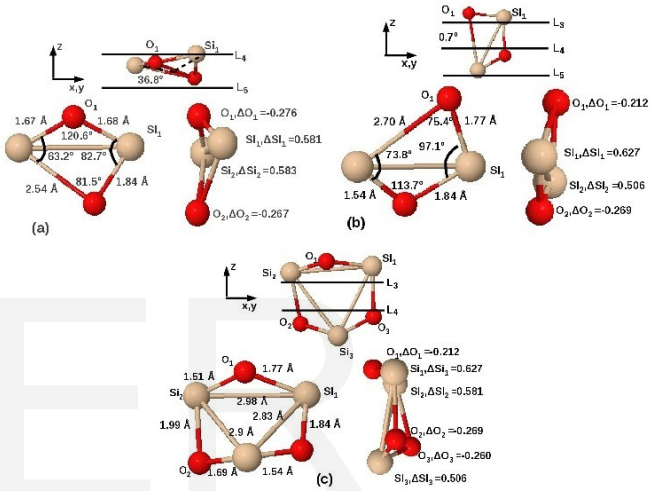

Fig. 4 (a) and (b) show the two-membered rings, and (c) the three-membered ring. Also, the magnitudes of the Si-O bonds (expressed in Å) and the O-Si-O interaction angles (in grades). Furthermore, the variation of the electronic charges of each of the atoms and the torsion angle, θ, expressed in grades, see text.

Now we will analyze the electronic density of states, see fig. 5, we notice that as the A_i's vary, the distributions only slightly move to the left, even though its general form is almost identical and with a band gap of 2 eV approximately (from -16 to -14 eV). The common characteristics of the DOS in fig. 5 result from the similar short-range order in the various forms of SiO_2 (the states of these SiO_2 systems are explicitly described in [31] and [32]). Besides, the band gap in SiO_2 systems is susceptible to the aspects of structural disorder and thermal vibrations[31], and as shown in this present work, also to the structural configuration of the system.

5 Conclusions

This work shows the relation between the topological and bond defects with electronic charge distribution of each the atoms that constitute to them, as the temperature varies, permitting a complete description of the system in function of the temperature (each A_i is related with a specific (average) tem-

perature). Both properties, structural and electronic, will permit us establish the rising of a global structure, and also for the association to the rings and the relation of these with the respective coordination (for example, this happens in our work starting from A_4). All according to the system tends to T_g.

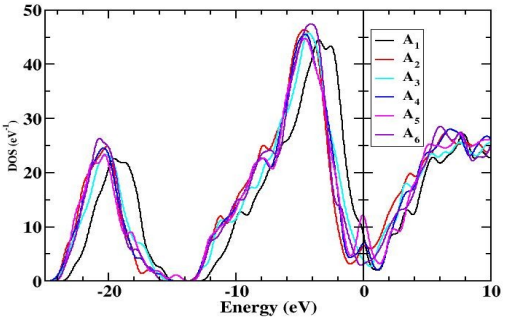

Fig. 5. The density of the electronic states (DOS) for the different A_i´s. (Calculated at the end of each run (after 0.27ps), see text.)

The dependency of the electronic density of states, in respect to the temperature indicates a gap of approximately 2 eV as the temperature varies. This is because a systematic relaxation was permitted to the system, and the influence of the structural configuration of it.

Therefore, the vital importance of the interaction between the structural and electronic properties is manifested, and the manner in which the system was obtained (the systematic and strategic way of applying fast cooling). All the previous can facilitate the predesign of the structural and electronic properties of the system for the specific objective. This last one is part of our next work.

REFERENCES

4 (a) The Physics of SiO_2 and its Interfaces, edited by S.T. Pantelides (Pergamon, New York, 1979); (b) A.P. Legrand, The Surface Properties of Silica, Wiley, New York, 1998; (c) R.B. Sosman, The Phases of Silica (Rutgers University, Piscataway, N. J., 1927); (d) L.Berthier and G. Biroli, Rev. Mod. Phys. **83**, 587 (2011).

5 T. Lopez, F. Figueras, J. Manjarrez, J. Bustos, M. Alvarez, J. Silvestre-Albero, F. Rodriguez-Reinoso, A. Martinez-Ferre, E. Martinez, Eur. J. Med. Chem. **45**, 1982 (2010).

6 R.B. Laughlin, J.D. Joannopoulus, C.A. Murray, K.J. Harnett, and T.J. Greytak, Phys. Rev. Lett. **40**, 461 (1978). M. L. Hair, Infrared Spectroscopy in Surface Chemistry (Dekker, New York, 1967).

7 M.L. Hair, Infrared Spectroscopy in Surface Chemistry (Dekker, New York, 1967).

8 B.P. Feuston and S.H. Garofalini, J. Chem. Phys. **89**, 5818 (1988).

9 B.P. Feuston and S.H. Garofalini, J. Chem. Phys. **91**(1), 564 (1989).

10 B.W.H. van Beest, G.J. Kramer, and R.A. van Santen, Phys. Rev. Lett. **64**, 1955 (1990).

11 J. Hutter, P. Ballone, M. Bernasconu, P. Focker, E. Fois, St. Goedecker, M. Parrinello, M. Tuckermann, CPMD, Version 3.3a, MPI für Festköperphysik and IBM Research, 1999-2000.

12 (a) C. Mischler, W. Kob, K. Binder, Comput. Phys. Comm. **147**, 222 (2002); (b) C. Mischler, J. Horbach, W. Kob, K. Binder, J. Phys.: Condens. Matter. **17**, 4005 (2005).

13 W. Kob, J. Phys.: Conden. Matter. **11**, R85 (1999).

14 C. A. Angell, Science, **267**, 1924 (1995).

15 M.T. Clavaguera-Mora, J. Thermal Anal. **35**, 1787 (1989).

16 R.G. Della Valle, H.C. Andersen, J. Chem. Phys. **97**(4),2682 (1992).

17 A. Cavagna, Phys. Reports 476, 51 (2009).

18 LAMMPS ("Large-scale Atomic/Molecular Massively Parallel Simulator") is a molecular dynamic program (free) from Sandia National Laboratories, the US Departament Energy Laboratory.

19 N. Trouiller, J.L. Martins, Phys. Rev. B **43**, 1993 (1991).

20 J.M. Soler, E. Artacho, J.D. Gale, A. Garcia, J. Junquera, P. Ordejón, D. Sanchez-Portal, J. Phys.: Condens. Matter. **14**, 2745 (2002).

21 User's Guide, SIESTA, version 3.2, (http://www.uam.es/siesta).

22 C. Fonseca Guerra, J.W. Handgraaf, E.J. Baerends, F.M. Bickelhaupt, J. Comput. Chem. **25**, 189 (2004).

23 G.W. Morey, The Properties of Glass (Reinhold, New York, 1960), pp. 221-293.

24 D. Cerosoli, M. Bernasconi, S. Iarlori, M. Parrinello, E. Tosatti, Phys. Rev. Lett. **84**, 3887 (2000).

25 H.C. Andersen, J. Chem. Phys. **72**, 2384 (1980).

26 J. Horbach, W. Kob, Phys. Rev. B **60**, 3169 (1999).

27 V.A. Bakaev, Phys. Rev. B **60**, 10723 (1999).

28 L. Verlet, Phys. Rev. **159**, 98 (1968).

29 L.V. Woodcock, C.A. Angell and P. Cheeseman, J. Chem. Phys. **65**, 1565 (1976).

30 (a) C. Lee, W. Yang, R.G. Parr, Phys. Rev. B **37**, 785 (1988); (b) J.P. Perdew, K. Burke and M. Ernzerhof, Phys. Rev. Lett. **77**, 3865 (1996).

31 M.T. Yin and M.L. Cohen, Phys. Rev. B **25**,7403 (1982).

32 An N-membered ring is defined as a closed ring of N-silicon atoms (or N-tetrahedra) connected by bridging oxygens.

33 A briding oxygen is the oxygen that two SiO_4 tetrahedra share in a cristal (vitreous) structure. A nonbridging oxygen is any other oxygen that is not shared by two tetrahedra.

34 J. Sarnthein, A. Pasquarello and R. Car, Phys. Rev. B **52**, 12690 (1995).

35 N. Binggeli, N. Troullier, José Luís Martins and J.R. Chelikowsky, Phys. Rev. B **44**, 4771 (1991).